CrystEngComm

PAPER

View Article Online
View Journal | View Issue

A facile synthesis of single crystal TiO_2 nanorods with reactive {100} facets and their enhanced photocatalytic activity†

Cite this: *CrystEngComm*, 2014, **16**, 3091

Yong Yang,[a] Guozhong Wang,*[a] Quan Deng,[a] Shenghong Kang,[a] Dickon H. L. Ng[b] and Huijun Zhao[ac]

Received 9th December 2013,
Accepted 26th January 2014

DOI: 10.1039/c3ce42505c

www.rsc.org/crystengcomm

High-energy {100} faceted single crystal TiO_2 nanorods were synthesized by a facile hydrothermal method. An interesting phase transition from the orthorhombic hydrogen titanate to anatase TiO_2 was observed during the reaction process. A structural formation model of the TiO_2 nanorods was proposed based on experimental evidence. The resultant {100} faceted TiO_2 nanorods exhibited considerably enhanced photocatalytic activity towards degradation of organic pollutants and removal of heavy metal ions owing to the special one-dimensional structure with the reactive {100} facets, thus showing a great potential in the field of water treatment. At the same time, the synthetic route provided guidance for the synthesis of high-energy {100} facets using EDTA and urea as effective modifiers. This approach may be extended to synthesize other functional oxide crystals with well-defined morphologies and to increase the percentages of certain exposed facets.

Introduction

As an important wide-band gap semiconductor, TiO_2 has been widely used for photocatalytic degradation of environmental pollutants.[1–5] Anatase phase TiO_2 has been demonstrated to be the most photocatalytically active among the various TiO_2 crystalline phases.[6,7] In addition to crystal phases, the exposed crystalline facet is also a critical factor affecting photocatalytic reactivity.[8] Unfortunately, the obtained anatase TiO_2 crystals are often dominated by the thermodynamically stable {101} facets due to the minimization of surface energy during the crystal growth process. Since Yang *et al.* demonstrated the fabrication of anatase TiO_2 with a large percentage of exposed {001} facets using hydrofluoric acid as a morphology controlling agent,[9] extensive efforts have been made to achieve the controlled synthesis of anatase TiO_2 with exposed high energy facets.[10–13] A pioneering work was reported by Li *et al.* in 2010 for synthesizing the tetragonal faceted-nanorods of anatase TiO_2 with exposed {100} facets.[14] Their fabrication involves the formation of Na-titanate nanotubes by hydrothermal treatment of P25 TiO_2 powder in NaOH solution and then hydrothermally transforming the Na-titanate nanotubes into the anatase phase of TiO_2 in basic solution. The resultant {100} faceted TiO_2 displays an enhanced photocatalytic activity. Thereafter, a number of approaches were reported for synthesizing anatase TiO_2 crystals with exposed {100} facets.[8,15–21] However, these reported methods either involve multiple complex reaction steps or require the use of expensive or extremely corrosive raw materials. Thus, the development of facile approaches to achieve controlled synthesis of a high energy {100} faceted anatase crystal under mild reaction conditions is highly desirable but challenging.

Herein, we report a facile hydrothermal route to achieve controlled synthesis of {100} faceted single crystal TiO_2 nanorods without the need for expensive, corrosive and toxic facet directing reagents. The inexpensive $Ti(SO_4)_2$ was used as the titanium source. The facet control was achieved by controlled release of Ti^{4+} using eco-friendly urea and ethylenediaminetetraacetic acid disodium salt (EDTA). To the best of our knowledge, this is the first time that the controlled growth of {100} faceted anatase TiO_2 is achieved under such mild conditions. A structural formation model was proposed based on experimental evidence. The photocatalytic activity of the TiO_2 nanorods was evaluated.

[a] *Key Laboratory of Materials Physics, Centre for Environmental and Energy Nanomaterials, Anhui Key Laboratory of Nanomaterials and Nanotechnology, Institute of Solid State Physics, Chinese Academy of Sciences, Hefei 230031, PR China. E-mail: gzhwang@issp.ac.cn; Fax: +86 551 6559 1434; Tel: +86 551 6559 5616*

[b] *Department of Physics, The Chinese University of Hong Kong, Shatin, Hong Kong*

[c] *Centre for Clean Environment and Energy, Gold Coast Campus, Griffith University, Queensland 4222, Australia*

† Electronic supplementary information (ESI) available: Additional figures, including the XRD crystallographic data, FESEM and TEM images, FT-IR spectra, and optical absorbance spectra. See DOI: 10.1039/c3ce42505c

Experimental section

Sample preparation

All reagents were commercially supplied and used without further purification. Chemicals used in this study were titanium sulfate ($Ti(SO_4)_2$, ≥96.0%, Shanghai Nanhui Chemical Reagent Co. Ltd, CP), urea ($CO(NH_2)_2$, ≥99.0%, Guoyao Chemical Reagent Co. Ltd, AR), ethylenediaminetetraacetic acid disodium salt (EDTA, Tian Jing Bei Fang Tian Yi Chemical Reagent Co. Ltd, AR). In a typical sample preparation, 2 mmol of $Ti(SO_4)_2$, 8 mmol of $CO(NH_2)_2$ and 0.8 g of EDTA were added to 40 mL deionized water. After stirring, the mixed suspension with a massive white precipitate was transferred to a 70 mL Teflon-lined autoclave and kept at 180 °C for 10 h before cooling down to room temperature. The white precipitate was collected, washed and rinsed with deionized water and ethanol, and then dried in an oven at 70 °C for 5 h. A series of experiments were conducted under different reaction conditions for comparison.

Characterization

X-ray diffraction (XRD) was performed using a Philips X'pert diffractometer with Ni-filtered monochromatic CuK_α radiation at 40 keV and 40 mA. The morphology and structure of the products were characterized using a field emission scanning electron microscope (FESEM, Sirion 200 FEI) with an accelerating voltage of 5.00 kV, and a transmission electron microscope (TEM, JEOL-2010, 200 kV) equipped with an energy dispersive X-ray spectrometer (EDX, Oxford, Link ISIS). The samples in the form of powder were ultrasonically dispersed in ethanol. The suspensions were dropped onto the SEM stub and the carbon grating for FESEM and TEM examinations, respectively. The photoluminescence (PL) measurement was performed using a LabRam confocal Raman microscope by the JY Company. Samples were excited by the 325 nm line of a continuous He–Cd laser at room temperature. The Fourier transform infrared spectrum (FT-IR) in the 4000–400 cm^{-1} region was characterized using a Thermo Nicolet NEXUS FT-IR spectrometer, with KBr as the diluent. The FT-IR characterization of the solution samples was as follows: different reagents (such as $Ti(SO_4)_2$ and EDTA) were dispersed in deionized water first, and then centrifuged to obtain the clear supernatant solution, afterwards a certain amount of the clear supernatant solution was added dropwise to the KBr substrate and then dried.

Photocatalytic activity evaluation

The photocatalytic degradation performance of the resultant TiO_2 nanorods was evaluated using degradation of methyl orange (MO) and methylene blue (MB) as the testing compounds. The photocatalytic degradation experiments were carried out by adding 40 mg of TiO_2 nanorods to 80 mL of MO or MB solution. Before irradiation, the sample solution was sonicated for 3 min and magnetically stirred under dark conditions for 30 min to establish adsorption/desorption equilibrium between the sample and the dye molecules and was then irradiated under UV light (300 W UV lamp) with a maximum emission at about 365 nm. After different time intervals of irradiation, 3.0 mL of treated sample was withdrawn and centrifuged before being analysed. A spectrophotometer (CARY-5E) was used to record the UV-vis absorption spectra of the centrifuged sample. As a comparison, experiments were also carried out to investigate the photocatalytic activity of the commercially available anatase phase TiO_2 powders (Aladdin Chemistry Co. Ltd, ≥99.8%). In another series of experiments, the evaluation of photocatalytic degradation of 50 ppm 2,4-dichlorophenoxyacetic acid (AR) and 10 ppm Cr(VI) in water was performed with similar procedures. $K_2Cr_2O_7$ (AR) was used as the Cr source. The concentration of 2,4-dichlorophenoxyacetic acid was determined based on the absorption peaks at 282 nm in UV-vis absorption spectra. The changes in the Cr(VI) concentration were determined by the spectrophotometric method using diphenylcarbazide to determine the absorbance of the solutions at a 540 nm wavelength using a UV-Vis spectrophotometer (CARY-5E).

Results and discussion

Structural characteristics

The X-ray diffraction pattern shown in Fig. S1 (see the ESI†) indicated that the as-synthesized product (at 180 °C for 10 h) was anatase phase TiO_2 (with space group: $I4_1/amd$, JCPDS no. 21-1272). The field emission scanning electron microscope (FESEM) images of the as-synthesized product suggest that the sample consists of TiO_2 nanorods with an average length of ~500 nm and a width of ~80 nm (Fig. 1a and b). The nanorods display well-defined lateral facets with sharp edges and the adjacent facets were perpendicular as well as with the same width (inset in Fig. 1a). This is further confirmed by the transmission electron microscopy (TEM) image

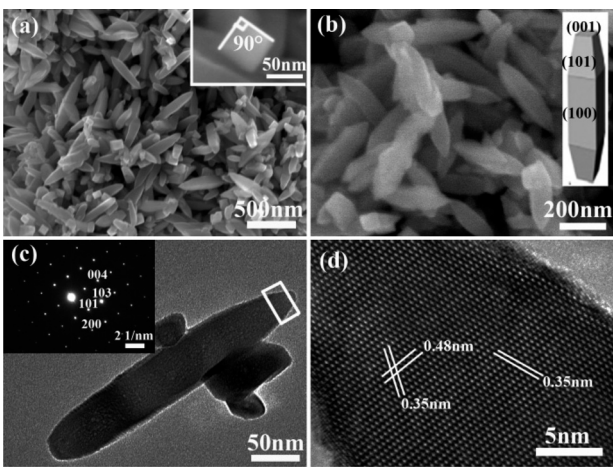

Fig. 1 (a and b) FESEM images of the TiO_2 nanorods, insets in (a) and (b) show the top view and schematic sketch of a single nanorod, respectively. (c) TEM image of an individual nanorod, inset is the corresponding SEAD pattern. (d) HRTEM image of the region highlighted by a rectangular box in part (c).

shown in Fig. 1c. The selected-area electron diffraction (SAED) and high-resolution TEM (HRTEM) were used to reveal the surface atomic structures. The SAED pattern in Fig. 1c (inset) shows diffraction spots of the [010] zone axis of anatase phase TiO_2. The HRTEM image in Fig. 1d shows three sets of lattice fringes with spacings of 0.48, 0.35 and 0.35 nm, which can be assigned to the {002}, {101} and {10$\bar{1}$} facets, respectively. The other part of the nanorod was further studied by TEM (Fig. S2 in the ESI†). The HRTEM image (Fig. S2b†) taken from the central area of an individual nanorod along the [1$\bar{1}$0] zone axis shows the {004} lattice fringes with a spacing of 0.24 nm.[15] Both the SEAD pattern and the HRTEM image suggested that the TiO_2 nanorods had a single crystalline structure of anatase phase with a growth direction along the [001] zone axis. The surface of these well-defined facets on the nanorods can be identified as dominant lateral {100}, {101} and a small part of top {001} planes (inset in Fig. 1b). This is in a good agreement with the reported results.[8,14] The percentage of high energy {100} facets estimated by the surface area of each facet from FESEM and TEM images was ~70%.

Controlled growth

To study the formation process, SEM images of samples from different reaction stages were taken (Fig. 2). When the precursors were mixed without heating, the massive white precipitate was formed in the solution (Fig. 2a). When the hydrothermal reaction was carried out at 180 °C for 5 min, the formation of randomly stacked nanoflakes was observed (Fig. 2b). When the reaction time was increased to 1 h, the nanoflakes became more obvious (Fig. 2c), along with some small rod-like nanoparticles (from the upper left corner of Fig. 2c). When the reaction proceeded for 3 h, the nanoflakes almost disappeared and many slender nanorods were observed (Fig. 2d). With further increase in reaction time to 5 h in the treatment, nanorods with well-defined facets can be observed, but there was also a small amount of nanoflakes in the products (inset in Fig. 2e). Pure TiO_2 nanorods with exposed high-energy {100} facets were obtained with 10 h reaction time (see Fig. 1). As the reaction time reached 15 h (Fig. 2f), the products were mainly in the form of mass nanorods along with some octahedral nanoparticles (inset in Fig. 2f). The corresponding XRD patterns of the products show an obvious phase transition that proceeded from the orthorhombic hydrogen titanate $H_2Ti_2O_5{\cdot}H_2O$ to anatase TiO_2 (Fig. S1a in the ESI†). Also, the change in peak intensity of the anatase TiO_2 indicated that the crystallization of the products increased with prolonged reaction time.

The reaction temperature was found to be critical for the formation of {100} faceted TiO_2 nanorods. Fig. 3 shows the FESEM images of the products subjected to a 10 h hydrothermal treatment under different temperatures. The self-supported radial nanoflakes can be observed in addition to some slender nanorods at 120 °C (Fig. 3a). The products were mainly in the form of slender nanorods along with a small amount of nanoflakes at 140 °C treatment temperature (Fig. 3b). The corresponding main XRD peaks of the two products could be indexed to anatase TiO_2 (see Fig. S1b in the ESI†), besides, there were also two small peaks which can be indexed as the orthorhombic $H_2Ti_2O_5{\cdot}H_2O$ phase. When the reaction temperature was further increased to 160 °C, the obtained products were anatase phase TiO_2 nanorods which are similar to the nanorods obtained at 180 °C (see Fig. 3c and S1b in the ESI†).

When the contrast experiment was done without the addition of urea while the other precursors remained the same, hydrothermal treatment at 180 °C for 1 h could not give hydrogen titanate nanoflakes or anatase TiO_2 nanorods, instead random aggregates of nanoparticles with unknown impurity phases were formed (Fig. S3 in the ESI†). When EDTA was not added and the other precursors were kept unchanged, the products were mainly microspheres composed of small anatase TiO_2 nanoparticles after hydrothermal treatment at 180 °C for 1 h (Fig. S4 in the ESI†).

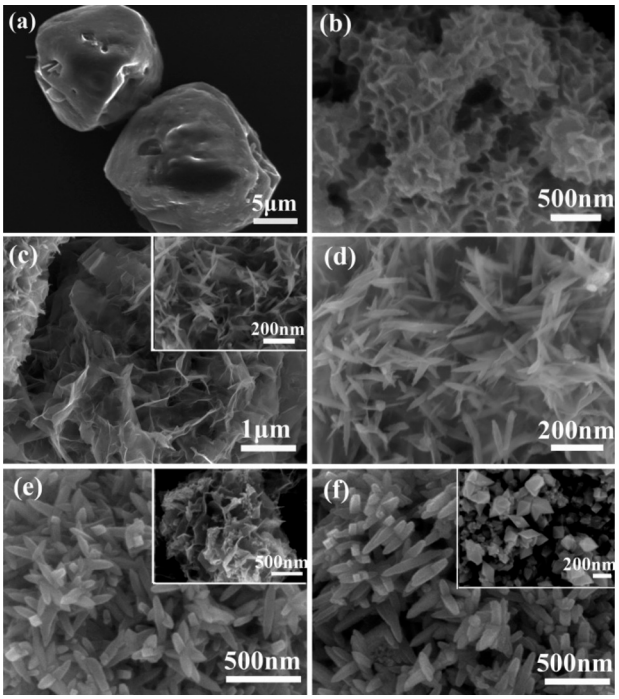

Fig. 2 FESEM images of samples subjected to 180 °C treatment for different times: (a) 0 min, (b) 5 min, (c) 1 h (inset is the enlarged image of the upper left corner of (c)), (d) 3 h, (e) 5 h and (f) 15 h (insets in (e) and (f) are the FESEM images of a small portion of the corresponding products).

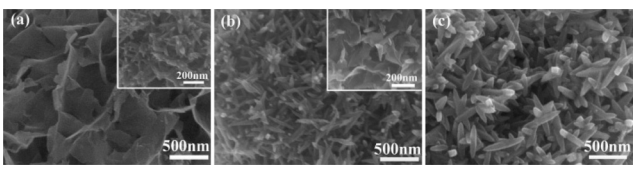

Fig. 3 FESEM images of the products obtained after 10 h hydrothermal treatment under different temperatures: (a) 120 °C; (b) 140 °C; (c) 160 °C. Insets in (a) and (b) are the FESEM images of a small portion of the corresponding products.

Based on the above experimental observations, the formation processes of the {100} faceted TiO_2 nanorods could be illustrated by Scheme 1, with possible reactions as shown below:

$$CO(NH_2)_2 + 3H_2O \rightarrow 2NH_4^+ + 2OH^- + CO_2 \quad (1)$$

$$[Ti(H_2O)(edta)] \rightarrow Ti^{4+} + EDTA + H_2O \quad (2)$$

$$2Ti^{4+} + 6H_2O \rightarrow H_2Ti_2O_5{\cdot}H_2O + 8H^+ \quad (3)$$

$$H_2Ti_2O_5{\cdot}H_2O \rightarrow 2TiO_2 + 2H_2O \quad (4)$$

Before hydrothermal treatment, the large aggregates in the precursor solution (Fig. 2a) were the stable chelating complexes of $[Ti(H_2O)(edta)]$ formed between Ti^{4+} and EDTA *via* the electrostatic attraction, which was confirmed by the FT-IR spectrum. The FT-IR peaks at 934, 1082, 1462, 1618, and 1697 cm^{-1} suggested the existence of the chelating complexes $[Ti(H_2O)(edta)]$ (Fig. S5a in the ESI†).[22,23] Pure EDTA solution had characteristic IR peaks at 1634 and 1392 cm^{-1} (curve 1 in Fig. S5b†), which can be attributed to the C=O stretching vibration.[23,24] When Ti^{4+} existed, the principal EDTA absorption peaks disappeared (curve 2 in Fig. S5b†), manifesting the formation of stable chelating complexes $[Ti(H_2O)(edta)]$ *via* $-COO^-$ groups.[24] However, the IR absorption peaks of EDTA still exist in the presence of urea (curve 3 in Fig. S5b†), implying that urea hardly reacted with EDTA.

As the reaction proceeds, $[Ti(H_2O)(edta)]$ would be dissociated and induced the formation of lamellar $H_2Ti_2O_5{\cdot}H_2O$ nanoflakes. The urea would decompose to give OH^- (reaction (1)) under hydrothermal conditions, which could be detected by the increasing pH of the reaction solution from the initial value of 1.87 to 4.21 after 5 min and 8.22 after 1 h under hydrothermal treatment (see Table 1 in the ESI†). It should be mentioned that the initial pH of the reaction solution was acidic, due to the precursor $Ti(SO_4)_2$ being a strong acid–weak base salt. It is well known that the pH of the aqueous solution of urea at room temperature was almost neutral. Therefore, adding urea into the $Ti(SO_4)_2$ solution or the mixed solution of $Ti(SO_4)_2$ and EDTA will not cause an obvious pH change (see Table 2 in the ESI†). This suggests that the effect of the decomposition of urea should be negligible at room temperature. However, accelerated urea decomposition under hydrothermal conditions releases OH^- and serves as an efficient pH controlling agent.

The chelating complexes $[Ti(H_2O)(edta)]$ were found to be stable below a pH value of 2.5 and would dissociate gradually to provide free Ti^{4+} species when pH is greater than 2.5 (reaction (2)).[25] Under hydrothermal treatment, the pH value of the reaction system increased due to the decomposition of urea, which would promote the dissociation of the chelating complexes $[Ti(H_2O)(edta)]$. Then, the gradually released free Ti^{4+} species would hydrolyze to form lamellar $H_2Ti_2O_5{\cdot}H_2O$ (reaction (3)),[26] which would further self-assembled into randomly stacked nanoflakes (Fig. 2b). The contrast experiment showed that urea was indeed essential in the reaction process (Fig. S3 in the ESI†). Also, Ti^{4+} species could be slowly released from $[Ti(H_2O)(edta)]$, effectively inhibiting the rapid growth of TiO_2 crystallites, facilitating the growth of Ti^{4+} into $H_2Ti_2O_5{\cdot}H_2O$ nanoflakes.[27] Without EDTA, the high concentration of free Ti^{4+} species in the reaction system would induce fast hydrolysis, nucleation and growth of TiO_2 crystallites instead of orthorhombic $H_2Ti_2O_5{\cdot}H_2O$ (Fig. S4 in the ESI†).[27] The results indicated that the Ti^{4+} concentration could be controlled by the chelating role of EDTA, which is essential for the formation of $H_2Ti_2O_5{\cdot}H_2O$ nanoflakes. This reaction step was similar to that of the reported formation process of the $LaCO_3OH$ nanosheet and nano-sized $BiVO_4$,[24,28] where the nucleation and growth processes of the products could be well controlled by the gradual release of La^{3+} and Bi^{3+} due to the chelating role of EDTA.

The $H_2Ti_2O_5{\cdot}H_2O$ nanoflakes are unstable under hydrothermal conditions and would be further dissolved and re-crystallized into TiO_2 anatase crystal nuclei with prolonged reaction time (reaction (4)).[8,14] Due to the difference in the adsorption stability of the capping reagents, the adsorbates would be adsorbed onto certain crystallographic planes more readily than the others, which would lower the surface energy of the bounded plane and hinder its growth. Theoretical analysis demonstrated that the hydroxyl could lower the surface free energy of the {100} facets,[8,14] leading to a decreased surface energy of the {100} facets to a level that is lower than that of {101} and {001} facets in the basic environment. This provides guidance for growing {100} facet-dominated anatase TiO_2. Our reaction system could provide this needed basic environment and pH could be well controlled around 9 (see Table 1 in the ESI†). Moreover, ammonia was easily dissolved or escaped in the solution, thus the pH value of the reaction solution was finely controlled in this reaction. Also, $EDTA^-$ had two $-NH_2$ and four $-COO^-$ groups which could act as a buffer agent to resist the excessive pH change of the reaction system.[29] In our reaction system, EDTA acts not only as a chelating agent to control the release of the Ti^{4+} species, but also as a pH buffer agent to ensure the needed basic condition for the growth of {100} facets. It is to note that the FT-IR characteristic peaks of EDTA re-appeared after hydrothermal reaction (curve 5 in Fig. S5b†), demonstrating that EDTA was indeed freed from

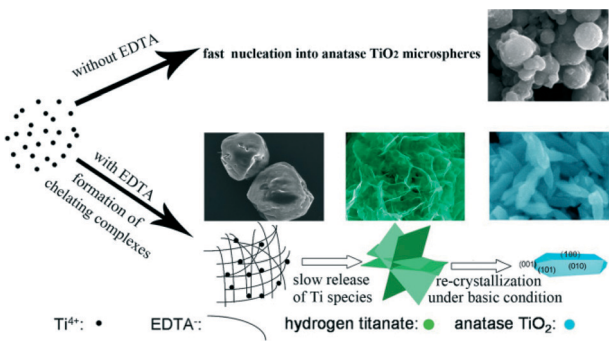

Scheme 1 A schematic illustration of a growth model for the formation of the TiO_2 nanorods.

the chelating complexes. When the reaction time was further increased to 15 h, the {100} facets became unstable due to their high reactivity, and some octahedral nanoparticles with lower energy {101} facets could be observed (inset in Fig. 2f).[21] When the reaction time was short (*e.g.* <5 h) or the reaction temperature was low (*e.g.* <160 °C), the $H_2Ti_2O_5{\cdot}H_2O$ nanoflakes could not be transformed into anatase TiO_2 completely, leading to the coexistence of the nanoflakes and nanorods.

Photocatalytic activity

The photocatalytic activity of {100} faceted TiO_2 nanorods was evaluated by the degradation of methyl orange (MO) and methylene blue (MB) under UV light irradiation. The intensities of the absorption peaks corresponding to MO at 464 nm and MB at 664 nm rapidly decreased with prolonged exposure time, and finally disappeared (Fig. S6 in the ESI†). For comparison, the photocatalytic activity of the commercial anatase TiO_2 powder was examined under the same experimental conditions (Fig. 4). The {100} faceted TiO_2 nanorods showed considerably enhanced photocatalytic activity towards both MO and MB when compared to the commercial TiO_2 powder. Considering the similar particle size (Fig. S7 in the ESI†) and BET specific surface area of the two TiO_2 photocatalysts (the BET specific surface area of the TiO_2 nanorods and commercial anatase TiO_2 powders were 3.1 and 2.2 $m^2\ g^{-1}$, respectively), the enhanced photocatalytic activity could be attributed to the presence of highly reactive {100} facets in the TiO_2 nanorods. PL emission spectra measurement was used to determine the charge recombination behavior and migration efficiency of the two TiO_2 photocatalysts.[30] The {100} faceted TiO_2 nanorods displayed a much weaker peak around 500 nm than that of the commercial TiO_2 powder (Fig. 5), indicating a lower charge carrier recombination rate, which might be due to the special one-dimensional structure with reactive {100} facets.[31]

Similar experiments using the TiO_2 nanorods for the degradation of 2,4-dichlorophenoxyacetic acid (a most widely used herbicide) and Cr(VI) (a typical heavy metal ion) in water were also conducted (Fig. S8 in the ESI†).[32,33] The results confirmed the superior photocatalytic activities of the {100} faceted TiO_2 nanorods towards the removal of persistent organic pollutants (POPs), 2,4-dichlorophenoxyacetic acid and heavy metal Cr(VI) ions.

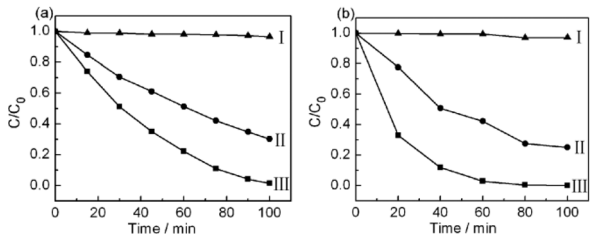

Fig. 4 (a) MO and (b) MB normalization concentrations *versus* the exposure time to UV light with different TiO_2 catalysts. Starting concentration C_0: 20 mg l^{-1}, C is the remaining concentration of MO or MB at time t. Curves I to III: without a photocatalyst, commercial TiO_2 powder and TiO_2 nanorods, respectively.

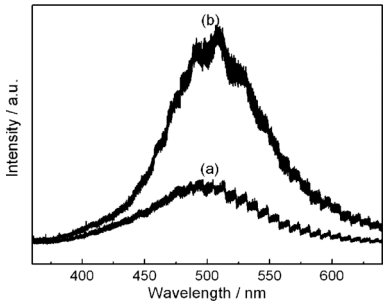

Fig. 5 Photoluminescence spectra of different TiO_2 samples: (a) TiO_2 nanorods and (b) commercial TiO_2 powder.

Conclusions

In summary, uniform single crystal anatase TiO_2 nanorods enclosed by reactive {100} facets were hydrothermally synthesized *via* the assistance of EDTA and urea. The method is simple and environmentally friendly that does not require the use of any corrosive and toxic reagents. The Ti species were slowly released and the pH value of the reaction system was well controlled by EDTA–urea, enabling the controlled growth of the nanorods with exposed high energy {100} facets. Furthermore, the anatase TiO_2 nanorods exhibited considerably enhanced photocatalytic activity towards both organic pollutants and heavy metal due to the special one-dimensional structure with reactive {100} facets. The synthetic route provided a useful guidance to achieve controlled growth of high-energy {100} facets under mild conditions, which might be applicable to the synthesis of other functional oxide crystals with well-defined morphologies and exposed high-energy facets.

Acknowledgements

This work was supported by the National Basic Research Program of China (grant no. 2013CB934302), the Natural Science Foundation of China (grant no. 51072199) and Strategic Priority Research Program of the Chinese Academy of Sciences (grant no. XDA09030200).

Notes and references

1 J. G. Yu, W. Liu and H. G. Yu, *Cryst. Growth Des.*, 2008, **8**, 930.
2 J. H. Xu, W. L. Dai, J. Li, Y. Cao, H. Li and K. Fan, *J. Photochem. Photobiol., A*, 2008, **195**, 284.
3 A. M. Luis, M. C. Neves, M. H. Mendonca and O. C. Monteiro, *Mater. Chem. Phys.*, 2011, **125**, 20.
4 J. Zhou, G. H. Tian, Y. J. Chen, J. Q. Wang, X. R. Cao, Y. H. Shi, K. Pan and H. G. Fu, *Dalton Trans.*, 2013, **42**, 11242.
5 W. Yan, F. He, S. L. Gai, P. Gao, Y. J. Chen and P. P. Yang, *J. Mater. Chem. A*, 2014, **2**, 3605.

6 F. Amano, T. Yasumoto, O. O. Prieto-Mahaney, S. Uchida, T. Shibayama and B. Ohtani, *Chem. Commun.*, 2009, 2311.
7 J. H. Pan, G. Han, R. Zhou and X. S. Zhao, *Chem. Commun.*, 2011, **47**, 6942.
8 J. Pan, X. Wu, L. Z. Wang, G. Liu, G. Q. Lub and H. M. Cheng, *Chem. Commun.*, 2011, **47**, 8361.
9 H. G. Yang, C. H. Sun, S. Z. Qiao, J. Zou, G. Liu, S. C. Smith, H. M. Cheng and G. Q. Lu, *Nature*, 2008, **453**, 638.
10 D. Q. Zhang, G. S. Li, X. F. Yang and J. C. Yu, *Chem. Commun.*, 2009, 4381.
11 Z. K. Zheng, B. B. Huang, X. Y. Qin, X. Y. Zhang, Y. Dai, M. H. Jiang, P. Wang and M. H. Whangbo, *Chem.–Eur. J.*, 2009, **15**, 12576.
12 H. M. Zhang, Y. H. Han, X. L. Liu, P. R. Liu, H. Yu, S. Q. Zhang, X. D. Yao and H. J. Zhao, *Chem. Commun.*, 2010, **46**, 8395.
13 G. L. Xiang, T. Y. Li and X. Wang, *Inorg. Chem.*, 2011, **50**, 6237.
14 J. M. Li and D. S. Xu, *Chem. Commun.*, 2010, **46**, 2301.
15 J. Pan, G. Liu, G. M. Lu and H. M. Cheng, *Angew. Chem.*, 2011, **195**, 2133.
16 X. W. Zhao, W. Z. Jin, J. G. Cai, J. F. Ye, Z. H. Li, Y. R. Ma, J. L. Xie and L. M. Qi, *Adv. Funct. Mater.*, 2011, **21**, 3554.
17 L. Wang, L. Zang, J. C. Zhao and C. Y. Wang, *Chem. Commun.*, 2012, **48**, 11736.
18 C. Z. Wen, H. B. Jiang, S. Z. Qiao, H. G. Yang and G. Q. Lu, *J. Mater. Chem.*, 2011, **21**, 7052.
19 J. Zhao, X. X. Zou, J. Su, P. P. Wang, L. J. Zhou and G. D. Li, *Dalton Trans.*, 2013, **42**, 4365.
20 H. Xu, S. X. Ouyang, P. Li, T. Kako and J. H. Ye, *ACS Appl. Mater. Interfaces*, 2013, **5**, 1348.
21 L. Q. Ye, J. Y. Liu, L. H. Tian, T. Y. Peng and L. Zan, *Appl. Catal., B*, 2013, **134**, 60.
22 M. Sato, H. Hara, T. Nishide and Y. Sawada, *J. Mater. Chem.*, 1996, **6**, 1767.
23 V. Etacheri, M. K. Seery, S. J. Hinder and S. C. Pillai, *Chem. Mater.*, 2010, **22**, 3843.
24 W. T. Sun, M. Z. Xie, L. Q. Jing, Y. B. Luan and H. G. Fu, *J. Solid State Chem.*, 2011, **184**, 3050.
25 P. D. Christy, N. Melikechi, N. S. N. Jothi, A. R. B. Suganthi and P. Sagayaraj, *J. Nanopart. Res.*, 2010, **12**, 2875.
26 H. Y. Zhu, X. P. Gao, Y. Lan, D. Y. Song, Y. X. Xi and J. C. Zhao, *J. Am. Chem. Soc.*, 2004, **126**, 8380.
27 H. Zhao, J. Z. Pan, S. Y. Du and C. H. Chen, *Bull. Mater. Sci.*, 2010, **33**, 427.
28 X. Y. Yang, Z. Zhai, L. Xu, M. Z. Li, Y. Zhang and W. H. Hou, *RSC Adv.*, 2013, **3**, 3907.
29 J. Glebska, A. Grzelak, L. Pulaski and G. Bartosz, *Anal. Biochem.*, 2002, **311**, 87.
30 C. Y. Su, L. Liu, M. Y. Zhang, Y. Zhang and C. L. Shao, *CrystEngComm*, 2012, **14**, 3989.
31 B. Poudel, W. Z. Wang, C. Dames, J. Y. Huang, S. Kunwar, D. Z. Wang, D. Banerjee, G. Chen and Z. F. Ren, *Nanotechnology*, 2005, **16**, 1935.
32 C. Guzman, G. del Angel, R. Gomez, F. Galindo-Hernandez and C. Angeles-Chavez, *Catal. Today*, 2011, **166**, 146.
33 J. K. Yang, S. M. Lee, M. Farrokhi, O. Giahi and M. S. Siboni, *Desalin. Water Treat.*, 2012, **46**, 375.

